PHOTONICS Research

One-order-higher Cr^{4+} conversion efficiency in Cr^{4+}:YAG transparent ceramics for a high-frequency passively *Q*-switched laser

Yingshuang Shan,[1] Le Zhang,[1,2,3,6] Tianyuan Zhou,[1,2] Cen Shao,[1] Lei Zhang,[4] Yuelong Ma,[1,5] Qing Yao,[1,5] Zhigang Jiang,[1,5] Farida A. Selim,[2] and Hao Chen[1,7]

[1]Jiangsu Key Laboratory of Advanced Laser Materials and Devices, School of Physics and Electronic Engineering, Jiangsu Normal University, Xuzhou 221116, China
[2]Department of Physics and Astronomy, Bowling Green State University, Bowling Green, Kentucky 43403, USA
[3]School of Materials Science and Engineering, Georgia Institute of Technology, Atlanta, Georgia 30332, USA
[4]SUSTech Academy for Advanced Interdisciplinary Studies, Southern University of Science and Technology, Shenzhen 518055, China
[5]School of Mechanical Engineering, Jiangsu University, Zhenjiang 212013, China
[6]e-mail: njutzl@163.com
[7]e-mail: chenhao@jsnu.edu.cn

Received 15 April 2019; revised 8 June 2019; accepted 18 June 2019; posted 19 June 2019 (Doc. ID 365093); published 1 August 2019

The Cr^{4+}-doped yttrium aluminum garnet (Cr^{4+}:YAG) saturable absorber, a new generation of passively *Q*-switched solid-state laser material, faces a significant obstacle of low conversion rate of chromium from trivalent to tetravalent, degrading efficiency in a passively *Q*-switched laser. In this paper, highly transparent Cr^{4+}:YAG ceramics were fabricated and committed to compare the laser performance with Cr^{4+}:YAG crystals on a 1 μm passively *Q*-switched laser. Thanks to the grain boundary effect, the Cr^{4+} conversion efficiency of 0.05 at.% Cr^{4+}:YAG transparent ceramics coated with high transparency (HT) films (T = 86.46% at 1064 nm) was nine times higher than that of 0.1 at.% Cr^{4+}:YAG single crystals coated with HT films (T = 84.00% at 1064 nm). Differing from the counterpart Cr^{4+}:YAG crystals, no absorption saturation tendency was observed for the 0.05 at.% Cr:YAG ceramics when the pump power exceeded ~1900 mW. Furthermore, the repetition frequency reached 217 kHz for 0.05 at.% Cr:YAG ceramics, which was a three-fold factor increase from that of the corresponding single crystal. The advantages of transparent ceramics over single crystals were proved through laser performance for the first time, to the best of our knowledge. This study also provided compelling evidence for replacing single crystals with ceramics for ultrafast dynamics.

https://doi.org/10.1364/PRJ.7.000933

1. INTRODUCTION

The *Q*-switched pulsed laser has extensive applications in remote sensing, target designation, laser guidance, laser medicine, laser marking, and other fields [1,2]. The *Q*-switched technology generally includes the actively *Q*-switched and passively *Q*-switched methods. The actively *Q*-switched laser requires external electrical equipment or mechanical control, and it is complicated in structure, relatively expensive, and large in volume [3,4]. As a result, an actively *Q*-switched laser has difficulty in achieving high pulse repetition frequency and high slope efficiency [5,6]. However, the passively *Q*-switched laser exhibits many advantages, such as low weight, simplicity of alignment, and operation without an external power supply or polarizing optics [7–9].

As a new generation of passively *Q*-switched solid-state laser material, Cr^{4+}-doped yttrium aluminum garnet (Cr^{4+}:YAG) has received great attention and has been rapidly developed due to its higher quantum efficiency, longer fluorescence lifetime, and better stability compared with organic dyes or color center crystals [10]. The excellent 1 μm passively *Q*-switched lasers are caused by the best overlap of the intrinsic absorption band of Cr^{4+} ions at 900–1200 nm with the emission peak of Nd^{3+} or Yb^{3+} ions [11,12]. Meanwhile, these two kinds of activator ions could be also co-doped into a Cr^{4+}:YAG lattice to obtain self-*Q*-switching lasers [13,14].

As the most important form, the Cr^{4+}:YAG single crystal was widely used for 1 μm passively *Q*-switched lasers in past years. In fact, the highest peak power could be generated by adjusting the pump beam waist incident on the Nd: YAG/Cr^{4+}:YAG composite crystal, and its power was over 235 kW [15]. Additionally, the properties of diode-pumped doubly *Q*-switched Nd:YAG laser with a Cr^{4+}:YAG saturable absorber and an acousto-optic modulator were first reported in Ref. [16]. Therefore, the application of a Cr^{4+}:YAG single

crystal for passively Q-switched lasers has been very mature. However, according to previous reports, only 0.1 at.% Cr^{4+} doping concentration and the low absorption coefficient of 2.7 cm^{-1} at 1.03 μm were achieved in YAG single crystals after air annealing [17]. As is known, this low doping concentration of Cr^{4+} was really caused by the low solid solubility of Cr^{4+} ions in the YAG lattice, and promoting more Cr^{3+} ions conversion into Cr^{4+} ions was an effective approach to enhancing the absorption coefficient. However, even after further prolonging the annealing time to 50 h at 1400°C in an oxygen atmosphere, the absorption coefficient at 1030 nm just reached 3.6 cm^{-1} in 10 at.% Yb^{3+}, 0.1 at.% Cr^{4+} co-doped YAG single crystal [18]. Therefore, in the YAG single crystal, the low solid solubility of Cr^{4+} ions and low Cr^{4+} conversion efficiency together restricted the output power and efficiency of Cr^{4+}:YAG-based 1 μm passively Q-switched lasers.

Nowadays, as another important laser gain material, transparent ceramics have many advantages over single crystals, such as flexibility for large size and composite structures, short production cycle, and cost saving. In fact, the biggest difference between ceramics and crystals is the existence of grain boundaries in ceramics [19,20]. The excessive doping ions were hardly doped into the YAG lattice during single crystal growth, while they could easily be incorporated into ceramics, even if there was a high possibility to distribute in grain boundaries. Then, the doping ions inside ceramics would retry to enter into the lattice site during the annealing process due to the effective release of grains stress, and further significantly enhance the solid solubility of doping ions [21]. In addition, as the fast diffusion pathway of atoms, the grain boundaries would greatly accelerate the oxygen transfer to oxidize Cr^{3+} into Cr^{4+} more effectively. Therefore, it is strongly speculated that the conversion rate of Cr^{4+} ions in Cr:YAG transparent ceramics is far higher than that of Cr:YAG crystals. However, there are very few studies to confirm the above conjectures until now.

In this paper, to verify our hypothesis, the Cr^{4+}:YAG transparent ceramics with excellent optical property were fabricated and employed to conduct the laser experiment to systematically compare with Cr^{4+}:YAG single crystals. As far as we know, this is the first study to exhibit the laser performance between Cr^{4+}:YAG ceramics and single crystals. The results showed that the conversion efficiency of Cr^{4+} ions in Cr:YAG ceramics was nearly one-order higher than that of Cr:YAG single crystals. The Cr^{4+}:YAG transparent ceramic is a considerable candidate for applications in 1 μm passively Q-switched lasers.

2. EXPERIMENTAL PROCEDURES

A. Ceramic Fabrication Experiment

Cr^{4+}:YAG transparent ceramics were fabricated by the solid-state reaction method, and the detailed processes were similar to those in our previous reports [15,22,23]. High-purity Y_2O_3 (99.99% purity; Alfa Aesar, Ward Hill, America), α-Al_2O_3 (99.99% purity; Sumitomo Chemicals, Tokyo, Japan), and Cr_2O_3 (99.99% purity, Alfa Aesar, Ward Hill, America) powders were selected as the starting materials. These powders were weighted precisely to result in a chromium content of 0.05 at.% and 0.1 at.% in the resultant Cr^{4+}:YAG ceramics $Y_3(Al_{1-x}Cr_x)_5O_{12}$. Divalent additives MgO (99.999% purity; Alfa Aesar, Ward Hill, America) and CaO (99.999% purity; Alfa Aesar, Ward Hill, America) powders were adopted as sintering aids and charge compensators. For all samples, based on our optimized results [24], the additional amounts of Ca^{2+} and Mg^{2+} were both kept at 0.1 mol.% according to Al^{3+} content, and the molar ratio between Ca and Mg was 1:1. The powder mixtures were ball milled in anhydrous ethyl alcohol for 15 h, and then the milled slurry was dried at 60°C for 36 h in an oven. After being sieved through a 200 mesh screen, the sieved powders were uniaxially pressed under 30 MPa in a stainless steel mold into pellets with a diameter of 16.0 mm, and the obtained pellets were further cold isostatic pressed (CIPed) at 200 MPa for 5 min. The CIPed green bodies were air calcined at 800°C for 6 h to remove the organic residues inside pellets. Then, the calcined green bodies were vacuum sintered at 1820°C for 8 h in a vacuum furnace under 10^{-4} Torr (1 Torr = 133.32 Pa) to obtain Cr:YAG transparent ceramics. After vacuum sintering, the as-sintered ceramics were air annealed at 1450°C in a muffle furnace for 10 h. Finally, all samples were ground and mirror polished on both surfaces, and their thicknesses were kept at 3 mm. For comparison, 0.1 at.% Cr:YAG single crystal (Hefei Ruijing Co., Ltd.) coated with high transparency (HT) films (T = 84.00% at 1064 nm) was used as a reference.

Microstructural investigations of the as-fabricated Cr^{4+}:YAG ceramics were conducted by a scanning electron microscope (SEM; JSM- 6510, JEOL, Kariya, Japan). A UV visible near-IR (UV-VIS-NIR) spectrophotometer (Lambda 950, Perkin Elmer, Waltham, America) was adopted to measure the in-line transmittance of the mirror polished Cr:YAG ceramics, and the scanning speed was 600 nm/min.

B. Laser Experiment

Figure 1 shows the schematic diagram of the laser experiment setup. The a-cut Nd:YVO_4 was chosen because its stimulated emission cross is four times higher than that of the c-cut one. The dimension of the Nd:YVO_4 slab as laser gain medium was 3.0 mm × 3.0 mm × 5.0 mm. It was coated with highly reflective (HR) at 1064 nm and antireflective film (AR) at 808 nm as a cavity mirror of the laser on the one end, and the other end was coated at AR 1064 nm to reduce the cavity loss. A concave mirror (φ = 200 mm, 97% AR at 1064 nm) was used as the output mirror (M2). The Cr^{4+}:YAG saturable absorber was placed near the Nd:YVO_4 slab. Before stepping the absorber into the cavity, we adapted the cavity to get a maximum CW transverse electromagnetic (TEM00) mode output power of 0.93 W at 1064 nm with a pump power of 2.14 W. An output coupler with 3% transmission was employed, and passively Q-switched pulses of Cr^{4+}:YAG with different initial

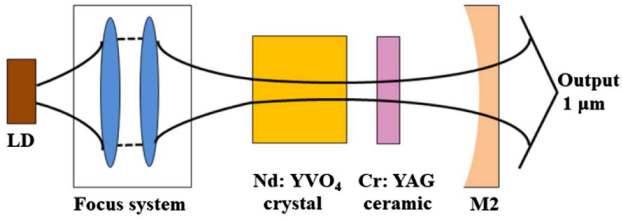

Fig. 1. Schematic diagram of the laser experiment.

transmissions were easily observed by using a positive-intrinsic-negative (PIN) photodiode and a digital oscilloscope. Besides, the optical spectra of the *Q*-switched laser were tested by the spectrum analyzer (AQ6370C, 600–1700 nm).

3. RESULTS AND DISCUSSION

Residual pores and grain boundary phases are generally considered as the main factors that affect the optical quality of transparent ceramics [22,23]. Figure 2 shows the SEM images of the Cr^{4+}:YAG transparent ceramics after thermal etching at 1450°C for 2 h. All ceramics exhibited a completely densified microstructure characterized by both transgranular and intragranular [Figs. 2(a) and 2(b)]. No pores or other scattering centers were detected, indicating the potentially high optical quality. Furthermore, it could be seen from the uniform surfaces in Figs. 2(c) and 2(d) that the grain size was similar at whatever Cr doping concentrations, and the mean size was approximately 2.0–3.0 μm in a very narrow distribution.

The photographs and the transmission spectrum of Cr^{4+}:YAG transparent ceramics with different Cr doping concentrations are depicted in Fig. 3. The transmittances of both Cr:YAG transparent ceramics at 1500 nm were higher than 84.0%, which was almost close to the theoretical value of YAG. Besides, the transmittance below 500 nm for both ceramics was nearly zero, owing to the strong absorption of the Cr^{4+} ion at this band. A broad absorption band ranging from 800 to 1200 nm centered at 1030 nm could also be observed from both ceramics. This absorption mainly corresponded to the $^3B_1(^3A_2) \rightarrow {}^3A_2(^3T_1)$ transition and was merely caused by the $^3B_1(^3A_2) \rightarrow {}^3E(^3T_2)$ transition of the tetrahedral Cr^{4+} ions. The absorption band centered at ~610 nm corresponded to the $^3B_1(^3A_2) \rightarrow {}^3E(^3T_1)$ transition of the Cr^{4+} ion [25]. Moreover, from the inset of Fig. 3, it is clear that both ceramics were fully transparent, and the letters behind the ceramics could be clearly resolved by the naked eyes. The color of the ceramics changed from light brown to dark brown, when the Cr doping concentrations increased from 0.05 at.% to 0.1 at.%.

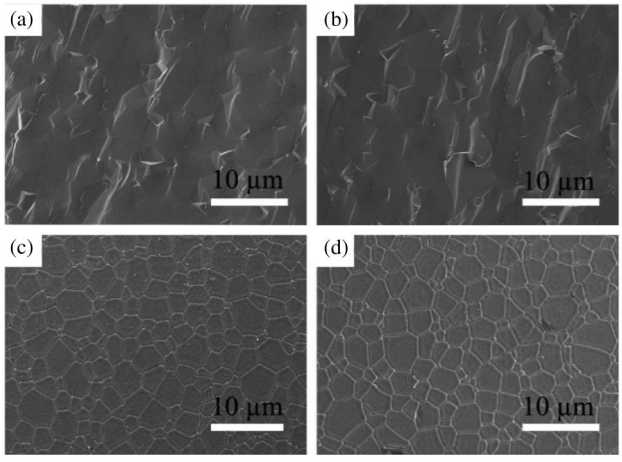

Fig. 2. SEM microstructures of facture surfaces of (a) 0.05 at.% and (b) 0.1 at.%, and the mirror-polished surfaces of (c) 0.05 at.% and (d) 0.1 at.% Cr^{4+}:YAG ceramics.

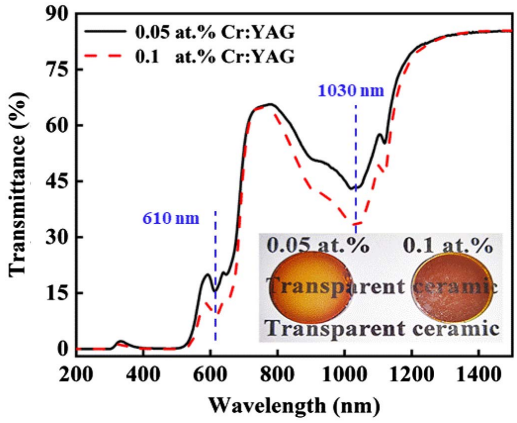

Fig. 3. In-line transmission spectra of the uncoated Cr:YAG transparent ceramics with different Cr doping concentrations.

The central wavelengths of the Cr^{4+}:YAG ceramics and single crystal lasers were both 1064 nm, confirmed by the spectrum analyzer (not shown here). The laser output power as a function of incident pump power is demonstrated in Fig. 4. Obviously, the laser property of Cr^{4+}:YAG ceramic was very close to that of Cr^{4+}:YAG crystal. By using the 0.05 at.% Cr^{4+}:YAG ceramic coated with HT films ($T = 86.46\%$ at 1064 nm) as the saturable absorber, a maximum output power of 100.8 mW at 1064 nm was obtained under an incident pump power of 2.14 W, with a threshold of 458.4 mW. For the 0.1 at.% Cr^{4+}:YAG transparent ceramic ($T = 85.84\%$ at 1064 nm), under an incident pump power of 2.14 W, a maximum output power and the laser threshold were 107.2 mW and 458.4 mW, respectively. Besides, for the corresponding Cr^{4+}:YAG single crystal, the output power of 114.9 mW was obtained under an incident power of 2.14 W. However, the observed threshold was as high as 731.2 mW, which was almost 1.5 times higher than that of Cr^{4+}:YAG ceramics. From Fig. 4, the slope efficiencies of the 0.05 at.%, 0.1 at.% Cr^{4+}:YAG transparent ceramics and 0.1 at.% Cr^{4+}:YAG crystal were 7.13%, 6.67%, and 10.54%, respectively. In addition, when the pump power was more than 910.4 mW, the pulse train of the 0.1 at.% Cr^{4+}:YAG ceramics was unstable, which was further illustrated in Fig. 5. It is speculated that the reason behind this was the emergence of multi-mode lasers [26].

Moreover, the pulse energy and peak power of Cr^{4+}:YAG single crystals were displayed in Figs. 5(a) and 5(b). Despite the increases of pulse energy and the peak power of Cr^{4+}:YAG single crystals being faster than those of ceramics, they tended to be saturated when the pump power was higher than ~1900 mW. The comparisons of pulse width and the repetition frequency of Cr^{4+}:YAG materials are also shown in Figs. 5(c) and 5(d). The pulse width of both Cr:YAG ceramics and crystals were almost similar at the level of 110 ns. However, it is surprising that the repetition frequency of the Cr:YAG ceramic was 217 kHz, which was three times higher than that of the corresponding single crystal (72 kHz). Therefore, Cr:YAG transparent ceramics prepared in this paper have great potential to improve the pulse energy and peak power by

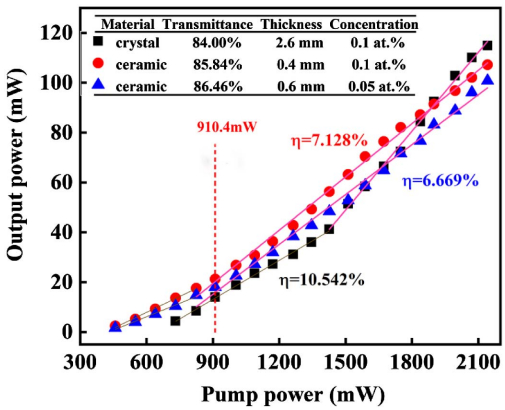

Fig. 4. Laser output power as a function of the pump power for Cr:YAG materials.

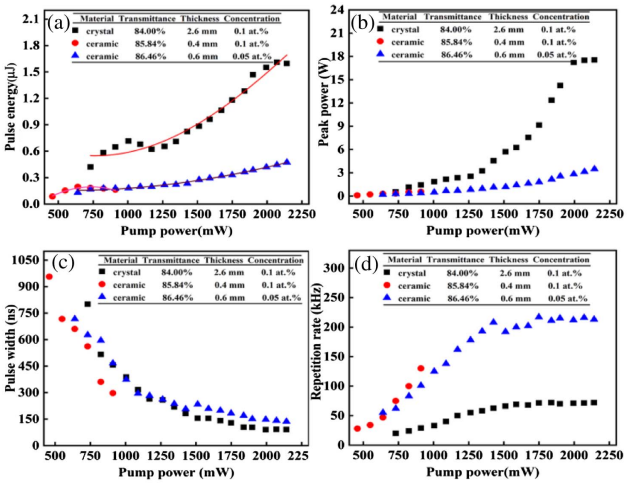

Fig. 5. Passively Q-switched laser property comparisons between transparent ceramics and single crystal: (a) pulse energy versus pump power; (b) peak power versus pump power; (c) pulse width versus pump power; (d) repetition frequency versus pump power.

further increasing the incident pump power [27]. It is noteworthy to see that the laser properties of the 0.05 at.% Cr^{4+}:YAG ceramic were similar, or even had an opportunity to surpass that of the 0.1 at.% Cr^{4+}:YAG crystals. This means the total amounts of effective Cr^{4+} ions were nearly the same for Cr^{4+}:YAG ceramic and single crystal. Assuming that the Cr doping concentration has no effect or a weak effect on the conversion efficiency of the Cr^{4+} ion, especially under the low doping concentration, the total amount of the converted Cr^{4+} ions in materials can be calculated by the following equation:

$$C_B \times Ah = n, \tag{1}$$

where C_B is the Cr doping concentration. h is the thickness of sample. n is the total amount of Cr^{4+} ions. A is the area of Cr^{4+}:YAG, and it is same for Cr^{4+}:YAG transparent ceramics and Cr^{4+}:YAG single crystals. Therefore, the total amounts of Cr^{4+} ions in Cr:YAG transparent ceramics (0.05 at.%, 0.6 mm) should be nine times higher than that in Cr:YAG single crystals (0.1 at.%, 2.6 mm). But, as shown above, the amounts of effective Cr^{4+} ions in these two materials were very close, and it is concluded that the conversion efficiency of Cr^{4+} ions per unit volume in 0.05 at.% Cr^{4+}:YAG transparent ceramics was about nine times higher than that of the 0.1 at.% Cr^{4+}:YAG single crystal. It also indicated that the difference in slope efficiency of the laser in Fig. 4 was caused by the total number of Cr^{4+} ions affected by sample thickness and doping concentration, not just by the transmittance of Cr^{4+}:YAG. This is an amazing result, and it has been quantitatively proved that the Cr^{4+} ion conversion efficiency in Cr^{4+}:YAG transparent ceramics was obviously higher than that of the single crystal for the first time, to the best of our knowledge.

In order to explain the reasons for the above phenomenon, a detailed analysis was carried out. To achieve a high conversion efficiency of the Cr^{4+} ion, the divalent additives (i.e., Ca^{2+} and Mg^{2+}) were used as charge compensators to regulate the charge state of the Cr ion in this study. The working mechanism is described as the following in Eqs. (2)–(4) [28]:

$$2MgO + 2Al_{Al}^{X} + O_{O}^{X} = 2Mg'_{Al} + V_{\ddot{O}} + Al_2O_3, \tag{2}$$

$$2CaO + 2Y_{Y}^{X} + O_{O}^{X} = 2Ca'_{Y} + V_{\ddot{O}} + Y_2O_3, \tag{3}$$

$$4Cr_{Al}^{X} + O_2 + 2V_{\ddot{O}} = 2O_{O}^{X} + 4Cr_{\dot{A}l}. \tag{4}$$

Although, for the Cr^{4+}:YAG single crystals, the divalent additives were also employed as charge compensators; it is difficult to solute a relatively high amount of divalent ions into the lattice by the conventional Czochralski method due to the limitation of the segregation coefficient [29]. As pointed out before, the existence of a grain boundary is a typical characteristic of ceramics. Doping cations with different ion radii would inevitably induce internal stress inside grains, which would be released by grain boundaries to a certain extent, and then increase the solubility of the divalent ions, leading to the enhanced conversion efficiency of Cr^{4+} ions in Cr:YAG transparent ceramics [Eqs. (2)–(4)]. The above phenomenon could be denoted as "grain boundary induced charge compensation effect", as seen in Fig. 6.

Besides the above effect, another reason that affects the conversion efficiency of the Cr^{4+} ion may be the "grain boundary accelerated oxidation effect". According to the Eq. (4), the trivalent Cr ions could be oxidized into the tetravalent state during the air annealing process, and the grain boundaries would provide rapid channels for the diffusion of oxygen atoms into ceramics in Fig. 6, making it easier to promote the conversion of Cr^{4+} ions, compared with that in single crystals. In fact, O_2 annealing was necessary to promote the Cr conversion from trivalent to tetravalent. In our experiment, even the divalent sintering additives have been employed in the fabrication of Cr:YAG transparent ceramics, where the dark brown color could have appeared just after vacuum sintering [28]. This phenomenon was in agreement with the reports about the fabrication of Cr:YAG single crystals [30], in which the color change just occurred after air annealing. Therefore, the one-order higher Cr^{4+} conversion efficiency in Cr:YAG transparent ceramics really resulted from the divalent sintering

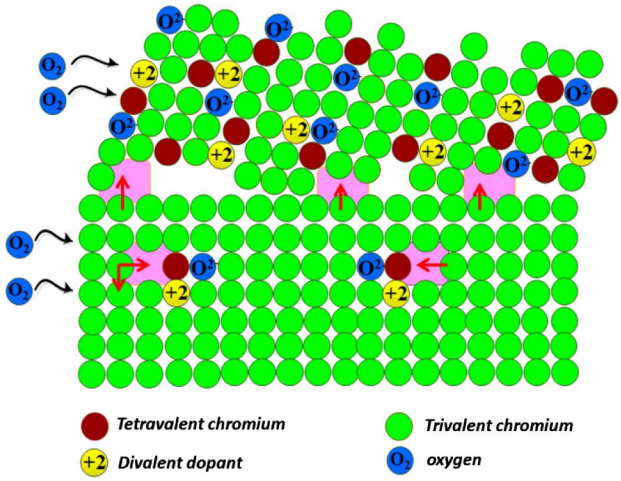

Fig. 6. Schematic diagram of the grain boundary effect in divalent-additives-doped Cr:YAG transparent ceramics.

additives and O_2 annealing under the assistance of grain boundaries, as shown in Fig. 6.

In addition, according to our previous report [24], by using divalent additives with small particle sizes, the conversion efficiency of the Cr^{4+} ion could be also promoted distinctly. Since fine divalent additives would be more inclined to distribute homogeneously at the micro level, the dissolution of divalent cations in the YAG lattice could be increased accordingly. Owing to the technical limitation, it is relatively hard to fabricate Cr:YAG single crystals with a homogeneous doping ion distribution by the conventional Czochralski method. On the contrary, the intrinsic feature of the ceramic powder mixing process provides the advantages mainly reflecting in the better uniformity of divalent additives in the powder mixture. It is beneficial for the conversion of tetravalent Cr ions in Cr:YAG transparent ceramics.

What is more, from Figs. 4 and 5, the laser performance between single crystals and ceramics was very similar, but the thicknesses of the prepared ceramics were much smaller than that of the single crystal. It is generally recognized that the heat dissipation problem for a laser system could be effectively mitigated if a thinner laser material is used. Besides, this also effectively facilitates the miniaturization of laser devices. Therefore, not only one-order-higher conversion efficiency of Cr^{4+} ion, but also one smaller and more integrated, laser device was achieved in Cr:YAG transparent ceramics instead of single crystals. In the following work, the nonlinear transmission of Cr:YAG transparent ceramics will be systematically studied. Furthermore, it can be expected that the potential application of transparent Cr:YAG ceramics-based *Q*-switched lasers is foreseen in the future [31,32], especially in the fields of medical treatment and industrial production due to the super-high repetition frequency observed in this study.

4. CONCLUSIONS

In this study, highly transparent Cr:YAG ceramics were successfully fabricated to achieve the passively *Q*-switched laser. Amazingly, for the 0.05 at.% Cr:YAG ceramics, the Cr^{4+} ion conversion per unit volume was nearly nine times higher than that of the 0.1 at.% Cr:YAG single crystal, due to the synergistic contributions of the "grain boundary induced charge compensation effect" and the "grain boundary accelerated oxidation effect." In addition, by using 0.05 at.% Cr^{4+}:YAG ceramics coated with HT films ($T = 86.46\%$ at 1064 nm) as the saturable absorber, a maximum output power of 100.8 mW at 1064 nm was obtained under an incident pump power of 2.14 W, with a threshold of 458.4 mW. The corresponding slope efficiency was 6.67%. Moreover, the repetition frequency of 0.05 at.% Cr^{4+}:YAG ceramics (217 kHz) was three times higher than that of corresponding crystals. The superiority of transparent ceramics over single crystals was proved by laser experiment for the first time, to the best of our knowledge. Therefore, Cr^{4+}:YAG transparent ceramics are a better saturable absorber for 1 μm passively *Q*-switched solid-state lasers than its single crystal counterpart. This study also provides a feasibility for the application of transparent ceramics in other fields, especially in the field of ultrafast dynamics (e.g., mode-locking laser).

Funding. National Natural Science Foundation of China (NSFC) (51402133, 51802142, 61603160, 61775088); Postgraduate Research Practice Innovation Program of Jiangsu Province (KYCX18_2096, KYCX18_2097, KYCX18_2098, KYCX18_2099); Special Project for Technology Innovation of Xuzhou City (KC16GZ014, KC16HQ236, KC16HQ237); Priority Academic Program Development of Jiangsu Higher Education Institutions (GRCK2017042411005977); Key Research and Development Project of Jiangsu Province (BE2018062, BE2019112).

Acknowledgment. Thanks to Professors Deyuan Shen and Wei Zhou for their thoughtful suggestions and discussions. We extend additional thanks to designer Cheng Wang for the graphical image.

REFERENCES

1. Q. Qian, D. Kong, S. Zhao, G. Li, X. Cheng, N. Wang, T. Li, D. Li, K. Yang, and J. Zang, "Promotion impact of thermal oxidation etching to saturable absorption performance of g-C_3N_4," Opt. Laser Technol. **111**, 597–603 (2019).
2. Z. Fan, J. Qiu, Z. Kang, Y. Chen, W. Ge, and X. Tang, "High beam quality 5 J, 200 Hz Nd:YAG laser system," Light Sci. Appl. **6**, e17004 (2017).
3. Y. Ma, H. Dang, F. Liu, X. Liu, F. Peng, S. Ding, and Q. Zhang, "Diode-pumped acousto-optically *Q*-switched laser using a novel Nd:$GdYTaO_4$ mixed crystal," J. Russ. Laser Res. **40**, 76–79 (2019).
4. N. Bawden, H. Matsukuma, O. Henderson-Sapir, E. Klantsataya, S. Tokita, and D. J. Ottaway, "Actively *Q*-switched dual-wavelength pumped Er^{3+}:ZBLAN fiber laser at 3.47 μm," Opt. Lett. **43**, 2724–2727 (2018).
5. Y. Shen, Y. Wang, K. Luan, H. Chen, M. Tao, and J. Si, "High peak power actively *Q*-switched mid-infrared fiber lasers at 3 μm," Appl. Phys. B **123**, 105 (2017).
6. D. Li, H. Xue, M. Qi, Y. Wang, S. Aksimsek, N. Chekurov, W. Kim, C. Li, J. Riikonen, and F. Ye, "Graphene actively *Q*-switched lasers," 2D Mater. **4**, 025095 (2017).
7. D. Mao, X. Cui, X. Gan, M. Li, W. Zhang, H. Lu, and J. Zhao, "Passively *Q*-switched and mode-locked fiber laser based on an ReS_2 saturable absorber," IEEE J. Sel. Top. Quantum **24**, 1100406 (2018).

8. Z. Kang, M. Liu, Z. Li, S. Li, Z. Jia, C. Liu, W. Qin, and G. Qin, "Passively *Q*-switched erbium doped fiber laser using a gold nanostars based saturable absorber," Photon. Res. **6**, 549–553 (2018).
9. L. Li, X. Yang, L. Zhou, W. Xie, Y. Wang, Y. Shen, Y. Yang, W. Yang, W. Wang, and Z. Lv, "Active/passive *Q*-switching operation of 2 μm Tm, Ho:YAP laser with an acousto-optical *Q*-switch/MoS_2 saturable absorber mirror," Photon. Res. **6**, 614–619 (2018).
10. S. Men, Z. Liu, Z. Cong, H. Rao, S. Zhang, Y. Liu, P. G. Zverev, V. A. Konyushkin, and X. Zhang, "High-repetition-rate widely tunable Li:F_2 color center lasers," Laser Phys. **26**, 025806 (2016).
11. B. Zhang, Y. Chen, P. Wang, Y. Wang, J. Liu, S. Hu, X. Xia, Y. Sang, H. Yuan, and X. Cai, "Direct bleaching of a Cr^{4+}:YAG saturable absorber in a passively *Q*-switched Nd:YAG laser," Appl. Opt. **57**, 4595–4600 (2018).
12. F. Lou, R. Zhao, J. He, Z. Jia, X. Su, Z. Wang, J. Hou, and B. Zhang, "Nanosecond-pulsed, dual-wavelength, passively *Q*-switched ytterbium-doped bulk laser based on few-layer MoS_2 saturable absorber," Photon. Res. **3**, A25–A29 (2015).
13. T. Zhou, L. Zhang, J. Zhang, H. Yang, P. Liu, Y. Chen, X. Qiao, and D. Tang, "Improved conversion efficiency of Cr^{4+} ions in Cr:YAG transparent ceramics by optimization the particle sizes of sintering aids," Opt. Mater. **50**, 11–14 (2015).
14. X. Guan, J. Wang, Y. Zhang, B. Xu, Z. Luo, H. Xu, Z. Cai, X. Xu, J. Zhang, and J. Xu, "Self-*Q*-switched and wavelength-tunable tungsten disulfide-based passively *Q*-switched Er:Y_2O_3 ceramic lasers," Photon. Res. **6**, 830–836 (2018).
15. C. Li and J. Dong, "Pump beam waist-dependent pulse energy generation in Nd:YAG/Cr:YAG passively *Q*-switched microchip laser," J. Mod. Opt. **63**, 1323–1330 (2016).
16. Z. Peng, Y. Ma, R. Yan, X. Li, H. Ying, Y. Xin, T. Yao, G. Lin, and L. Jiang, "Doubly *Q*-switched Nd:YAG ceramic laser," J. Russ. Laser Res. **39**, 187–191 (2018).
17. X. Xu, Z. Zhao, P. Song, G. Zhou, J. Xu, and P. Deng, "Effects of growth atmosphere, annealing temperature, Cr content, and Ca/Cr ratio on the Cr^{4+} absorption of Cr, Yb:YAG crystals," J. Opt. Soc. Am. B **21**, 1289–1293 (2004).
18. J. Dong, P. Deng, X. U. Jun, and F. Gan, "Investigation of absorption spectra of (Cr^{4+}, Yb^{3+}):YAG crystal," Chin. J. Lasers B **8**, 475–510 (1999).
19. B. Sun, L. Zhang, T. Zhou, C. Shao, L. Zhang, Y. Ma, Q. Yao, Z. Jiang, F. A. Selim, and H. Chen, "Protected-annealing regulated defects to improve optical properties and luminescence performance of Ce:YAG transparent ceramics for white LEDs," J. Mater. Chem. C **7**, 4057–4065 (2019).
20. L. Zhang, J. Wu, P. Stepanov, M. Haseman, T. Zhou, D. Winarski, P. Saadatkia, and S. Agarwal, "Defects and solarization in YAG transparent ceramics," Photon. Res. **7**, 549–557 (2019).
21. K. Vikrant and R. E. García, "Charged grain boundary transitions in ionic ceramics for energy applications," NPJ Comput. Mater. **5**, 24 (2019).
22. M. Graf, M. Lihter, M. Thakur, V. Georgiou, J. Topolancik, B. R. Ilic, K. Liu, J. Feng, Y. Astier, and A. Radenovic, "Fabrication and practical applications of molybdenum disulfide nanopores," Nat. Protoc. **14**, 1130–1168 (2019).
23. K. Balasubramanian, T. Biswas, P. Ghosh, S. Suran, A. Mishra, R. Mishra, R. Sachan, M. Jain, M. Varma, and R. Pratap, "Reversible defect engineering in graphene grain boundaries," Nat. Commun. **10**, 1090 (2019).
24. T. Zhou, L. Zhang, Z. Li, S. Wei, J. Wu, L. Wang, H. Yang, Z. Fu, H. Chen, C. Wong, and Q. Zhang, "Enhanced conversion efficiency of Cr^{4+} ion in Cr:YAG transparent ceramic by optimizing the annealing process and doping concentration," J. Alloys Compd. **703**, 34–39 (2017).
25. X. Chen, Y. Wu, Z. Lu, N. Wei, J. Qi, Y. Shi, T. Hua, Q. Zeng, W. Guo, and T. Lu, "Assessment of conversion efficiency of Cr^{4+} ions by aliovalent cation additives in Cr:YAG ceramic for edge cladding," J. Am. Ceram. Soc. **101**, 5098–5109 (2018).
26. K. Shortiss, M. Shayesteh, W. Cotter, A. H. Perrott, M. Dernaika, and F. H. Peters, "Mode suppression in injection locked multi-mode and single-mode lasers for optical demultiplexing," Photonics **6**, 27 (2019).
27. M. R. Shcherbakov, K. Werner, Z. Fan, N. Talisa, E. Chowdhury, and G. Shvets, "Photon acceleration and tunable broadband harmonics generation in nonlinear time-dependent metasurfaces," Nat. Commun. **10**, 1345 (2019).
28. T. Zhou, L. Zhang, C. Shao, B. Sun, W. Bu, H. Yang, H. Chen, F. A. Selim, and Q. Zhang, "Sintering additives regulated Cr ion charge state in Cr doped YAG transparent ceramics," Ceram. Int. **44**, 13820–13826 (2018).
29. D. Krishnakumar and N. P. Rajesh, "Growth and optical characterization of europium and cerium doped KCl single crystals by Czochralski method for dosimetric applications," J. Electron. Mater. **48**, 1629–1633 (2019).
30. Y. Wu, J. Li, F. Qiu, Y. Pan, Q. Liu, and J. Guo, "Fabrication of transparent Yb, Cr:YAG ceramics by a solid-state reaction method," Ceram. Int. **32**, 785–788 (2006).
31. S. Omori, "Development of a lens-less mid-infrared laser head for the optical fiber tip oscillation to apply to therapeutic treatment," IEEJ Trans. Electron. Inf. Syst. **137**, 561–564 (2018).
32. J. M. Serres, P. Loiko, X. Mateos, J. Liu, H. Zhang, K. Yumashev, U. Griebner, V. Petrov, M. Aguiló, and F. Díaz, "Multi-watt passively *Q*-switched Yb:YAB/Cr:YAG microchip lasers," Proc. SPIE **10082**, 100820T (2017).